

TRANSFER FUNCTION ESTIMATION FOR SPACEBORNE TELESCOPES

G. Le Besnerais and L. M. Mugnier

Office National d'Études et de Recherches Aérospatiales, B.P. 72, F-92322 Châtillon cedex, France

ABSTRACT

The on-orbit calibration of the transfer function (TF) of a spaceborne optical telescope is of paramount importance for the restoration of its recorded images. We propose a novel method based on a physical modeling of the TF and on the automatic extraction from the image of sub-images containing appropriate patterns such as step functions. A least-square criterion is computed with all the extracted sub-images, and is minimized as a function of the unknowns, which are the TF parameters and the step parameters. Our simulation results validate the method and show a precise estimation of the full 2D TF.

1. INTRODUCTION

The on-orbit calibration of the transfer function (TF) of a spaceborne telescope may be performed using resolution targets, but this reduces the time available for observations. Methods not needing the acquisition of such special purpose images are thus preferable. Yet, estimating the TF from a single image is a difficult problem akin to blind deconvolution (BD), as both the TF and the object are unknown.

BD usually considers the TF characteristics as nuisance parameters and aims at restoring the observed object, while the situation is reversed for on-orbit calibration. In BD the object modeling (by, e.g., a Markov random field) yields many object parameters to be estimated (usually pixel values). Additionally, the PSF or TF modeling is often rather crude and not physically motivated (e.g., a 3×3 pixel PSF).

In order to obtain a good precision on the TF estimation, we instead choose to extract and use sub-images in which the object can be described by simple parametric models, e.g., step functions, similarly to [1, 2]. Additionally, we propose to use a physical modeling of the TF. It is parameterized by the optical aberrations of the instrument, which are expanded on (a limited number of) Zernike polynomials, as proposed for the BD of turbulence-degraded images [3].

Section 1 is devoted to the principle of the TF estimation method from a set of selected sub-images. Section 2 validates the estimation method by means of simulations. Section 3 discusses the automatic selection of suitable sub-images from the whole image. Section 4 illustrates the performance of the complete extraction plus estimation process on a realistic simulated image.

2. TRANSFER FUNCTION ESTIMATION

2.1. Observation model

We assume that the recorded image i is the noisy sampled convolution of the observed object o (Earth scene) with the instrument's PSF h :

$$i = [h \star o]_{\text{III}} + n, \quad (1)$$

where $[\cdot]_{\text{III}}$ denotes the sampling operator.

The instrument is assumed to be partially known. Its TF \tilde{h} is modeled as the product of the (known) detector transfer function (DTF) \tilde{h}_{det} with the optical transfer function (OTF) \tilde{h}_{opt} :

$$\tilde{h} = \tilde{h}_{\text{opt}} \times \tilde{h}_{\text{det}}. \quad (2)$$

The OTF is modeled through the aberrations (or phase) φ in the instrument's pupil [4] expanded on the first Zernike polynomials Z_l : $\varphi(x, y) = \sum_{l=4}^{\infty} a_l Z_l(x, y)$. Indeed in a space telescope there are essentially low order aberrations, which we here limit to Zernike polynomials Z_4 (defocus) to Z_{11} (spherical aberration). The unknown of interest is the OTF but these aberrations allow us to parameterize the latter with few, physically meaningful coefficients. Assuming that the spectral bandwidth is small compared to the central wavelength, the OTF is related to the aberrations in the pupil through [4]:

$$\tilde{h}_{\text{opt}} = \text{FT} \left(|\text{FT}^{-1}(P(x, y)e^{j\varphi(x, y)})|^2 \right), \quad (3)$$

where P is the pupil (or aperture) function, and FT denotes the Fourier transform. Lastly, the ratio f_c/f_n of the OTF's cutoff to the detector's Nyquist frequency is assumed to be known, and will be taken as 1 in the following.

2.2. Considered sub-images

The TF estimation is performed on sub-images which should have a high frequency (HF) content, accept a simple parametric model, and be sufficiently numerous in an image to lead to a reasonable statistical contrast. Linear features such as step functions meet all these conditions and are the ones used herein.

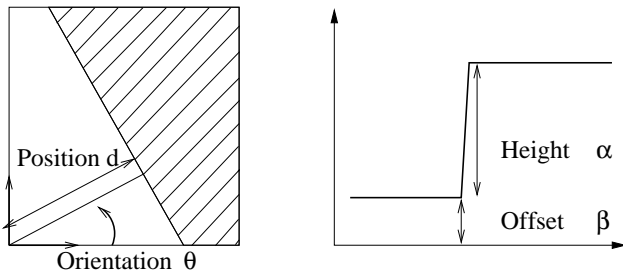


Fig. 1. Parameters of a step function: position and orientation (left), height and offset (right).

2.3. Principle of the transfer function estimation

We start with a set of K sub-images $i_1, \dots, i_k, \dots, i_K$, whose support S_K may be very different. These sub-images each correspond to an object which is assumed to be a step (or Heavyside) function. This object, denoted by o_k , is fully characterized by its orientation θ_k , its distance to the origin d_k , its height α_k and its lower value (or offset) β_k , as illustrated on Fig. 1.

Because the estimation of the OTF boils down to that of the first aberrations, we shall denote the PSF by $h(\{a_l\}_{l=4}^{11})$. The estimation is performed by minimizing a least square criterion, which is non-linear in the aberrations:

$$J(\{a_l\}, \{\theta_k, d_k, \alpha_k, \beta_k\}) = \sum_{k=1}^K \sum_{(p,q) \in S_k} |i_k(p, q) - [h(\{a_l\}_{l=4}^{11}) \star o_k(\theta_k, d_k, \alpha_k, \beta_k)](p, q)|^2. \quad (4)$$

This criterion measures the discrepancy between the sub-image models $[h \star o_k]_{\text{III}}$ and the sub-images i_k extracted from the recorded image i . In the case of a stationary white Gaussian noise, which is a reasonable approximation for satellite imaging, minimizing this criterion is equivalent to searching for a maximum likelihood solution.

2.4. Minimization of the criterion

The criterion is minimized jointly in all parameters, which are the aberrations and the object parameters, globally for all sub-images.

An essential step of the minimization of the criterion is its computation, which is essentially that of a sub-image model $[h \star o_k]_{\text{III}}$ for the current parameters. The computation of h is easily performed by using eqs. (2) and (3) and by replacing the FT by an FFT in the latter. We use the Radon (“Fourier slice”) theorem to reduce the computation burden of the criterion to 1D computations. Indeed, the following properties can easily be derived: firstly, the image of an object which is a linear feature (in particular a 2D step function) is linear too, and results from the spreading of a

1D image profile along the direction of the linear feature. Secondly, this image profile in turn is the 1D convolution of an object profile with the line spread function (LSF). Lastly, the LSF is the 1D inverse Fourier transform of a cut of the 2D transfer function.

The minimization is accelerated both by analytic considerations and by reasonable approximations. Firstly, the criterion is quadratic in any (α_k, β_k) , so that it can be minimized analytically in these variables, as a function of the other unknowns. Secondly, we have checked that the angles θ_k can be estimated precisely without knowing the aberrations, *i.e.*, with a perfect PSF. To do this, we minimize criterion J as a function of all (θ_k, d_k) for null aberrations. One notices that the minimization can be performed separately on each variable pair (θ_k, d_k) because each only appears in the k -th term of J .

Thanks to these considerations, the criterion to be minimized then only contains the variables of interest a_l that are related to the OTF, and the distances d_k . Indeed, these must be re-estimated because they code for the step positions, which depend on the shape of the PSF. The minimization is achieved by means of the Powell method, which does not need the analytic expression of the criterion’s gradient.

3. VALIDATION OF THE ESTIMATION METHOD ON SYNTHETIC IMAGES

A first validation of the method was to estimate the OTF on sub-images that were computed as mentioned above by making use of the Radon theorem; the results are very good, but probably not representative of the estimation quality attainable on more realistic images.

In the following, the sub-images are 32×32 and computed by the discrete convolution of an oversampled object with an oversampled PSF, which approximates a continuous convolution and is then sampled appropriately. Thus, a simulated sub-image is not computed in the same way as the corresponding sub-image model during the estimation. This aims at validating the robustness of the estimation with respect to small modeling errors and at preparing the validation on more realistic images such as the one presented in Section 5.

The OTF is defined through the 8 first Zernike polynomials, with aberration coefficients that make up a total phase variation of $2\pi/8$ rd RMS. The DTF is that of a CCD detector and takes into account the temporal integration along the satellite track. The global transfer function and its two (optical and detector) components are represented on Fig. 2.

We first present simulation results with noiseless images. Even with only two sub-images oriented at 0 and 90° , the estimated transfer function is very good in these directions (see Fig. 3). It is very poor in other directions, with a maximum error of 0.10; this illustrates the fact that each

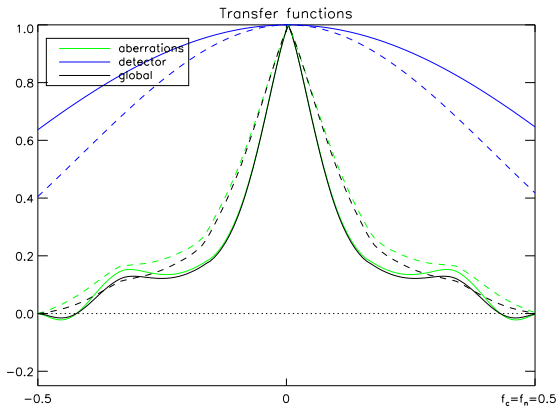


Fig. 2. Transfer function used for the simulations, obtained as product of the optical TF by the detector TF. Profiles along x in solid line, along y in dashed line.

# of sub-images	2	4	8
Maximum error	$10.2 \cdot 10^{-2}$	$2.6 \cdot 10^{-2}$	$2.0 \cdot 10^{-2}$
MSE	$2.1 \cdot 10^{-2}$	$0.49 \cdot 10^{-2}$	$0.41 \cdot 10^{-2}$

Table 1. Maximum error and mean-square error (MSE) on the transfer function estimation for two, four and eight noiseless sub-images.

sub-image of a step provides information in one direction, perpendicular to the step. When the number of sub-images increases while the steps' orientations diversify, the estimation quickly improves. Table 1 summarizes the transfer function estimation results for two, four and eight noiseless sub-images, with regularly spaced orientations. In particular for eight sub-images the maximum estimation error over the whole spatial frequency domain is 0.02.

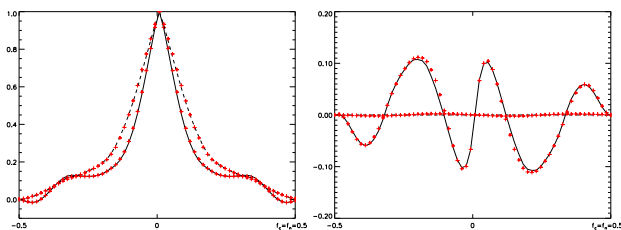


Fig. 3. Profiles of the true (— along x , --- along y) and estimated (+++) transfer functions from two noiseless sub-images. Left: real part; right: imaginary part.

We now consider eight sub-images with the same orientations as above, and assess the robustness of the method with respect to noise. For this purpose, the sub-images are degraded by an additive stationary white Gaussian noise of standard deviation σ_n , and the transfer function is estimated from these eight sub-images. The considered values of σ_n

σ_n	0%	1%	3.2%	10%
Max. error	$2.0 \cdot 10^{-2}$	$2.0 \cdot 10^{-2}$	$2.0 \cdot 10^{-2}$	$5.8 \cdot 10^{-2}$
MSE	$0.41 \cdot 10^{-2}$	$0.41 \cdot 10^{-2}$	$0.46 \cdot 10^{-2}$	$0.99 \cdot 10^{-2}$

Table 2. Maximum error and mean-square error (MSE) on the transfer function estimation for eight sub-images with varying noise levels. The noise is stationary white Gaussian, with a standard deviation of 0%, 1%, $\sqrt{10}$ % and 10% of the image maximum value respectively.

are 1%, $\sqrt{10} \approx 3\%$ and 10% of the image maximum value. The first value is typical of an Earth observing telescope, the second one is a more noisy case, and the third one is an extreme case.

Up to a value of $\sigma_n = 3\%$, the estimation quality remains almost constant and the maximum error does not exceed 2% (see Table 2). For 10% noise, the error becomes very important and more sub-images would be needed to reach a reasonable maximum error value.

4. AUTOMATIC EXTRACTION OF THE SUB-IMAGES

The extraction is achieved in two steps. In the first step we select sub-images which meet the following conditions: firstly, the extension of any sub-image both along the step and orthogonally to it should be greater than the assumed PSF diameter d ; in the following we use $d = 20$ pixels. Secondly, $|m_1 - m_2| > 2 * \max(s_1, s_2)$, where m_1, m_2 denote the mean values and s_1, s_2 the standard deviations of the two regions separated by the edge. For these purposes, we use a standard edge detector followed by a polygonalization step and by a region growing segmentation starting on both sides of the edges that are long enough.

The second step further checks the sub-images for consistency with the model of a convolved and noisy step function. This step is akin to sub-pixel localization of edges, as already noted by Bones *et al.* [2].

Each sub-image is rotated so that the edge is aligned with the vertical axis, using the orientation given by the polygonalization step. Then two tests are conducted on the resulting (horizontal) profiles. Firstly, the variations in each profile near both ends should be consistent with the image SNR. The sub-image is rejected if these variations are above $2\sigma_n$. Secondly, the central part of the profiles should be close to the mean profile but may be shifted because the orientation is only approximately known at this stage. We compute by a least-square fit a shift for each profile, in order to precisely align the edge with the vertical axis. A linear regression step is conducted on the vector of shifts, and the sub-image is rejected if the residual shift standard deviation is above a given threshold. In the following we use a threshold of 0.1 pixel.

5. VALIDATION OF THE GLOBAL METHOD ON A REALISTIC IMAGE

We have used an aerial 1704×1704 metric image of the Grenoble region (©IGN) to generate the object by a radiometric transformation that sharpened the edges. We could not use the original image itself as an object; indeed, this image was already somewhat smooth because of its acquisition process. A 426×426 4m resolution image of this object is obtained by discrete convolution (see the discussion in Sect. 3). The PSF is the same as that of Sect. 3, and the standard deviation of the added noise is 1%.

Figure 4 shows the image and the 12 sub-images resulting from the extraction. The result of the transfer function estimation is presented in Fig. 5. The maximum error is $2.5 \cdot 10^{-2}$, and is only reached for frequencies for which no sub-image provides information.



Fig. 4. Test image and extracted sub-images.

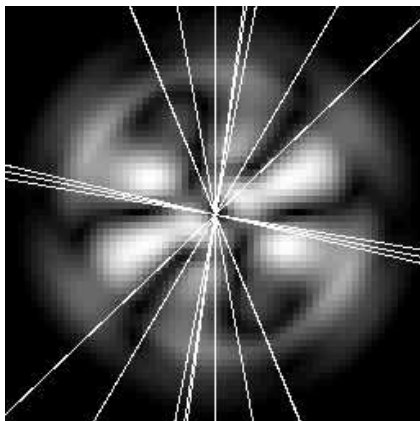


Fig. 5. Modulus of the difference between the true transfer function and its estimate. The maximum value is $2.5 \cdot 10^{-2}$. The lines indicate the directions orthogonal to the edges of the selected sub-images.

6. CONCLUSION

A novel method has been presented for the identification of the transfer function of an optical telescope from a single image. This method can be used both for the performance assessment of the instrument after launch and for the restoration of the images recorded by the instrument. This method is based on: (1) a physical modeling of the TF via the optical aberrations of the instrument; (2) the extraction of sub-images containing features such as natural step functions that can be parameterized easily; (3) the global transfer function estimation from the set of all sub-images by a least-square criterion minimization which is non-linear in the unknown aberrations.

The estimation part of this method has first been validated on simulated sub-images of step functions. Then, the complete sub-image extraction and transfer function estimation procedure has been validated on a realistic image. Future work include:

- taking into account other features, such as lines and double edges, to increase the number of useful sub-images;
- validating the method on undersampled images. It is intrinsically suitable for such images, but the undersampling should still yield some degradation of the performance, because the PSF of an undersampled image is coded with less pixels;
- the automatic tuning of some of the threshold parameters for the extraction and selection of the sub-images. These parameters should depend on system parameters such as f_c/f_n and the image SNR.

The authors thank F. Champagnat for fruitful discussions.

7. REFERENCES

- [1] B. Forster and P. Best, “Estimation of SPOT P-mode point spread function and derivation of a deconvolution filter,” *Journal of Photogrammetry and Remote Sensing*, vol. 49, pp. 32–42, 1994.
- [2] P. J. Bones, T. Bretschneider, C. J. Forne, R. P. Millane, and S. J. McNeill, “Tomographic blur identification using image edges,” in *Image Reconstruction from Incomplete Data*, 2000, vol. 4123.
- [3] T. J. Schulz, “Multiframe blind deconvolution of astronomical images,” *J. Opt. Soc. Am. A*, vol. 10, no. 5, pp. 1064–1073, 1993.
- [4] M. Born and E. Wolf, *Principles of Optics*, Pergamon Press, Sixth (corrected) edition, 1993.